

NASA Contractor Report 4206

# A General Method for Unsteady Heat Transfer on Turbine Blades

Tuncer Cebeci  
*California State University  
Long Beach, California*

Max F. Platzer  
*Naval Postgraduate School  
Monterey, California*

Prepared for  
Lewis Research Center  
under Purchase Order C-80017-F



National Aeronautics  
and Space Administration

**Scientific and Technical  
Information Division**

**1989**

## A GENERAL METHOD FOR UNSTEADY HEAT TRANSFER ON TURBINE BLADES

by

Tuncer Cebeci\* and Max F. Platzer\*\*

### SUMMARY

This report is concerned with the development of a general method for calculating unsteady heat transfer on turbine blades. It is based on the numerical solution of the boundary-layer equations for laminar, transitional and turbulent flows. A novel procedure has been developed to account for the movement of the stagnation point caused by blade-passing wakes and has been applied to the stagnation region of three model flows with results which confirm its validity for laminar flows. It has also been applied to an experimental arrangement in which the average Nusselt number has been reported for turbulent flows and the results show considerable promise.

---

\*Professor and Chairman, Aerospace Engineering Department, California State University, Long Beach, CA.

\*\*Professor, Department of Aeronautics, Naval Postgraduate School, Monterey, CA.

PRECEDING PAGE BLANK NOT FILMED

## TABLE OF CONTENTS

	<u>Page</u>
1.0 Introduction . . . . .	1
2.0 Basic Equations . . . . .	5
2.1 Turbulence Model . . . . .	5
2.2 Initial and Upstream Conditions . . . . .	7
2.3 Transformed Equations . . . . .	8
3.0 Numerical Method . . . . .	10
3.1 Regular Box Scheme . . . . .	10
3.2 Characteristic Box Scheme . . . . .	12
4.0 Results and Discussion . . . . .	17
4.1 Oscillating Airfoil Model . . . . .	17
4.2 Gust Response Model . . . . .	20
4.3 Rotor Wake Model . . . . .	22
5.0 Concluding Remarks . . . . .	27
5.0 References . . . . .	28
Appendix. External Velocity Distribution in the Stagnation Region with Nonuniform Onset Flow . . . . .	A-1

## 1.0 INTRODUCTION

Gas turbine designers are constantly expanding the pressure and temperature operating thresholds of modern turbines in order to achieve greater power densities. This in turn requires careful thermal-structural analysis in order to ensure that these turbines, which deliver such excellent performance, will also run for a long time before maintenance is required. The costs associated with hot section maintenance account for approximately 60 percent of total aircraft engine maintenance [1] and the turbine industry is aggressively pursuing programs to improve the predictability of turbine life [2]. In addition, NASA has a durability technology program, known as the Hot Section Technology (HOST) project [3,4] directed at improving the predictive tools for analyzing aircraft gas turbines and another program directed at improvement of the durability of the Space Shuttle Main Engine (SSME) [5].

The ability to predict the metal temperature distribution is a key factor in life prediction. Coincident with the beginning of the HOST project, Stepka [6] estimated that the ability to predict steady-state metal temperature in an operating engine was within 100K, and that this could be refined to 50K by testing prototypes. This level of thermal accuracy is estimated to lead to an order of magnitude uncertainty in life prediction [7].

Periodic reviews of gas turbine heat transfer [8-10] suggest that progress is being made in measuring and analyzing the complex flows associated with steady-state heat transfer in gas turbines. Research on unsteady heat transfer in turbine passages is, however, just beginning to appear. It is premature to evaluate the effects of wake-generated unsteady heat transfer on turbine durability but the research data to provide the necessary thermomechanical loads are emerging rapidly [11-20] with most of the information of aerodynamic properties acquired in large low-speed turbines. Dring, et al. [11] explored the nature of the boundary-layer response to turbine wakes and the unsteady pressure loading using thin-film surface sensors. Hodson [13] and Binder, et al. [14] mapped the convection of wakes through the rotor and flow properties in a rotor at 8850 rpm have also been reported in [14].

The nature of the blade-passing problem can be explained in relation to Fig. 1a which shows that the rotor blade passes through the wake of the upstream

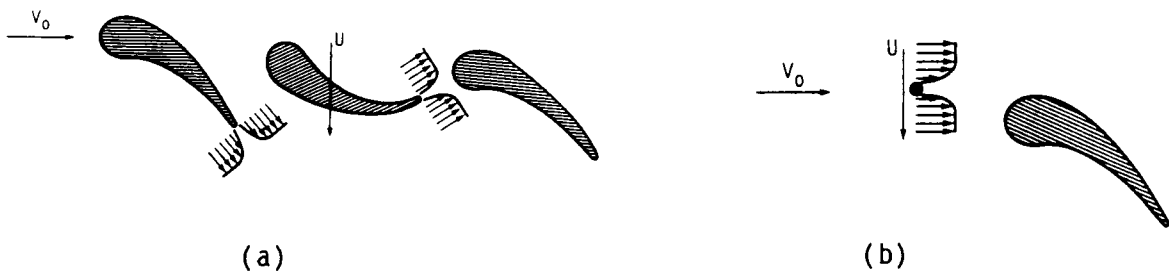


Figure 1. Flow configuration. (a) Turbine stage. (b) Simulation.

stator blade and generates a wake which affects the onset flow to the second stator. In effect, the blades of the rotor and second stator are subjected to a freestream velocity which varies periodically with time and with a random turbulence fluctuation superimposed. These effects may be simulated by the arrangement of Fig. 1b which shows one cylinder of a number arranged on a wheel which rotates upstream of a turbine blade.

Most relevant heat-transfer data have been obtained in short-duration facilities [15-18] or by using short duration techniques [19,20]. Thin-film resistance thermometers provide information of surface temperature and are combined with a one-dimensional semi-infinite heat-conduction analysis to yield time-resolved heat flux. Dunn and coworkers have pioneered this technique and, in their most recent work [15,16], have begun to obtain time-resolved heat flux data in a real turbine stage at fully-scaled conditions. At the University of Oxford [17,18], rotor wakes are simulated with a spoked wheel rotating in front of a linear cascade and the results show that the wakes impinging on the airfoil can cause the local boundary layer to undergo transition and reverse transition at the frequency of the passing wakes. O'Brien et al. [19] used the transient technique in a steady-running rig, also with a spoked wheel wake generator, and showed that the time-average of the time-resolved heat transfer agreed closely with conventional steady-state data. Morehouse and Simoneau [20], used the same rig, see Fig. 2, and showed that it was necessary to separate the heat transfer effects due to the unsteady disturbances of periodic wakes from those generated by conventional turbulence.

The recent advances in computational fluid dynamics have made it possible to predict blade pressure distributions, detailed boundary-layer and wake profiles, skin-friction and heat-transfer coefficients by solving the steady, full Navier-Stokes equations, see for example Shamroth [21]. Also Rai

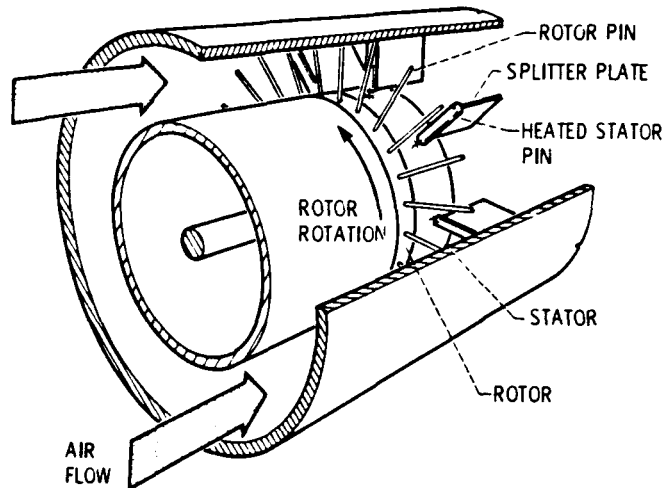


Figure 2. Experimental set-up of O'Brien et al. [19].

[22] has attempted to reproduce Dring's measurements by constructing a Navier-Stokes computer code with a complex arrangement of patched and overlaid grids. Navier-Stokes solutions have the advantage of enabling the prediction of both attached and separated viscous flows and hence can be expected to become a valuable engineering method as soon as computation times can be reduced and questions concerning the computational accuracy can be resolved.

In this report an alternative approach is pursued which has proven reliable and powerful in many external flows. It is based on the use of interactive boundary-layer theory which requires the development of viscous and inviscid methods and their coupling by special techniques such as those described in [23-26]. The inviscid method must be able to cope with the periodic onset velocities of Fig. 1b and their effects on the blade flow from the stagnation region to wake. The boundary-layer method for the resulting unsteady flows has to account for the reversals associated with the movement of the stagnation point with time and space as well as flow reversals and separation that may occur in the downstream region. The problem of flow reversal can be solved without interaction between inviscid and viscous flow solutions but a special numerical procedure is required to deal with the changing flow direction.

The work described here is directed towards the development of a general method for calculating unsteady heat transfer on turbine blades. As an essential preliminary we describe a general boundary layer method for calculating heat transfer for prescribed freestream conditions and test it for three model

problems which emphasize the stagnation region. We assume that the external velocity distribution is represented by a function

$$u_e(x,t)/u_\infty = A(\xi,t)[\xi - B(t)] \quad (1)$$

which allows the variation of the stagnation point and the freestream velocity. The first model problem corresponds to flow over a thin ellipse in a constant freestream velocity field with a uniform wall temperature and with a local external velocity which changes with angle of attack. The second model problem corresponds to an initially steady flow which accelerates from  $u_e/u_\infty = \xi$  at  $t = 0$  to  $u_e/u_\infty = 2(\xi - 1)$  at large times with corresponding movement of the stagnation point from 0 to 1. The third model problem corresponds to the flow of [20], see Fig. 2, in which the flow over a circular cylinder with a uniform wall temperature is subjected to an external velocity distribution which changes with time due to the interference of a series of cylinders which are attached to a rotating wheel. Measurements of local flow properties and of wall heat transfer have been reported in [20] and allow quantitative assessment of the calculation method.

The basic equations, initial and boundary conditions are considered in the following section which is followed by a description of the numerical method used to solve the boundary-layer equations. Section 4 presents the results and discussion and the report ends with a summary of the more important conclusions.

## 2.0 BASIC EQUATIONS

For two-dimensional, incompressible time-dependent laminar and turbulent flows, the boundary-layer equations and their boundary conditions are well known. For specified wall temperature, no mass transfer and with eddy viscosity,  $\epsilon_m^+$ , and turbulent Prandtl number,  $Pr_t$ , concepts they can be written in the form [27]:

$$\frac{\partial u}{\partial x} + \frac{\partial v}{\partial y} = 0 \quad (2)$$

$$\frac{\partial u}{\partial t} + u \frac{\partial u}{\partial x} + v \frac{\partial u}{\partial y} = \frac{\partial u_e}{\partial t} + u_e \frac{\partial u_e}{\partial x} + v \frac{\partial}{\partial y} (b_1 \frac{\partial u}{\partial y}) \quad (3)$$

$$\frac{\partial T}{\partial t} + u \frac{\partial T}{\partial x} + v \frac{\partial T}{\partial y} = \frac{v}{Pr} \frac{\partial}{\partial y} (b_2 \frac{\partial T}{\partial y}) \quad (4)$$

$$y = 0, \quad u = v = 0, \quad T = T_w(x) \quad (5a)$$

$$y = \delta, \quad u = u_e(x, t), \quad T = T_e \quad (5b)$$

$$b_1 = 1 + \epsilon_m^+, \quad b_2 = 1 + \frac{Pr}{Pr_t} \epsilon_m^+, \quad \epsilon_m^+ = \epsilon_m / \nu \quad (6)$$

### 2.1 Turbulence Model

The presence of  $\epsilon_m^+$  in  $b_1$  and  $b_2$  and  $Pr_t$  in  $b_2$  requires a turbulence model and various expressions can be used for this purpose. The choice lies between an algebraic formulation in which detailed flow features, including transition from laminar and turbulent flow, are represented semi-empirically and models where the transport of turbulence properties is facilitated by differential equations. The models of the latter type, including the ubiquitous  $k-\epsilon$  model, offer the possibility of some degree of generality but, so far, have been unable to deal with low Reynolds number phenomena. Since the representation of transition is essential to the present problem, we have preferred to use the algebraic eddy-viscosity approach of Cebeci and Smith, which is known to represent transition adequately. The formulation is given by a two-layer model defined by

$$\epsilon_m = \begin{cases} \{0.4y[1 - \exp(-y/A)]\}^2 \left| \frac{\partial u}{\partial y} \right| \gamma_{tr} & 0 \leq y \leq y_c \\ 0.0168 \left| \int_0^\infty (u_e - u) dy \right| \gamma_{tr} \gamma & y_c \leq y \leq \delta \end{cases} \quad (7a)$$

$$(7b)$$

where

$$A = 26\nu u_\tau^{-1}, \quad u_\tau = \left( \frac{\tau_w}{\rho} \right)^{1/2}, \quad \gamma = \frac{1}{1 + 5.5(y/\delta)^6} \quad (8)$$

The condition used to define  $y_c$  is the continuity of the eddy viscosity; from the wall outward, Eq. (7a) is applied until its value is equal to that given by Eq. (7b).

In Eq. (7),  $\gamma_{tr}$  is an intermittency factor which accounts for the transitional region that exists between a laminar and turbulent flow. It is given by

$$\gamma_{tr} = 1 - \exp\left[-G(x - x_{tr}) \int_{x_{tr}}^x \frac{dx}{u_e}\right] \quad (9)$$

Here  $x_{tr}$  is the location of the start of transition and the empirical factor  $G$  is

$$G = \frac{1}{1200} \frac{u_e^3}{\nu^2} R_{x_{tr}}^{-1.34} \quad (10)$$

where the transition Reynolds number  $R_{x_{tr}} = (u_e x/\nu)_{tr}$ .

Equation (9) has been determined in terms of flows where the freestream turbulence was characterized by low intensities and small scale. Its extension to turbine blade passages which are subject to onset flows with turbulence intensities in excess of 15% and scales larger than the width of the blade passage imply that modifications may be required. The flow of Ref. [20] involves a freestream intensity in excess of 1% and intensities of 10% in the near wakes of the circular cylinder which were used to simulate blade passing flows. As a consequence of the above, the influence of  $\gamma_{tr}$  must be determined empirically and with consideration of these high turbulence flows.

## 2.2 Initial and Upstream Conditions

The determination of the initial conditions required for the above system is important and sometimes can be arbitrary but in that event, the values of  $\partial u/\partial t$  at  $t = 0$  are nonzero; this implies an inviscid acceleration and, as a consequence, a slip velocity develops at the wall and is smoothed by an inner boundary layer initially of thickness  $(\nu t)^{1/2}$  in which viscous forces are important. Thus a double structure develops in the boundary layer and may be treated by the numerical method described in [28]. However, if interest is centered on the solution at large times, this feature may be reduced in importance by requiring that the initial velocity distribution satisfies the steady-state equation with the instantaneous external velocity. In addition, it is necessary to smooth the external velocity  $u_e(x,t)$  so that  $\partial u_e/\partial t = 0$  at  $t = 0$  and standard numerical methods may be used and remain stable. The use of a smoothing function introduces some loss of accuracy at small values of  $t$  but the error soon decays to zero as the required value of  $u_e$  is approached.

The calculation of upstream boundary conditions in the  $(t,y)$  plane at some  $x = x_0$  when the conditions at a previous time line are known, can introduce different problems. To illustrate these difficulties for the case of a moving stagnation point, let us consider Eq. (1). Since  $u_e = 0$  at the stagnation point by definition, its location,  $x_s$ , based on the external streamlines is given by

$$x_s = A(x_s, t) \quad (16)$$

Figure 3 shows the variation of the stagnation point with time according to Eq. (1) with  $B(t) = 1 + c \sin \omega t$ ,  $c = 1$ ,  $\omega = \pi/4$ . We see that the stagnation point  $x_s$  is at 2 when  $t = 2$  and at 0 when  $t = 6$ , etc. If  $x_s$  were fixed, we could assume that  $u = 0$  at  $x_s = 1$  for all time and for all  $\eta$ , but this is not the case. It is also possible to assume that the stagnation point is coincident with zero  $u$ -velocity for a prescribed time but we should note that the stagnation point given by Eq. (16) is based on vanishing external velocity. For a time-dependent flow, as we shall discuss later, this does not necessarily imply that the  $u$ -velocity is zero across the layer for a given  $\xi$ -location and specified time; flow reversals do occur due to the movement of the stagnation

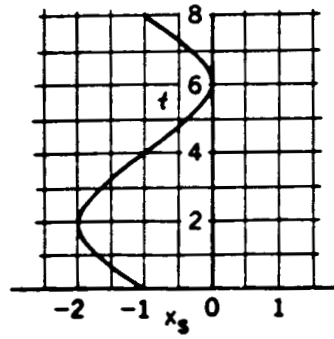


Figure 3. Variation of the stagnation point with time according to Eq. (1).

point and cause the locus of zero  $u$ -velocity to vary with  $x$  requiring the use of a special numerical method, as will be discussed in Section 3.

### 2.3 Transformed Equations

It is more convenient and useful to express Eqs. (2)-(5) in a form more suitable for computation. To achieve this, we define the dimensionless variables  $\tau$ ,  $\xi$ ,  $\eta$ ,  $w$ ,  $m$ ,  $G$  together with a dimensionless stream function  $f$ ,

$$\tau = \frac{tu_0}{L}, \quad \xi = \frac{x}{L}, \quad \eta = \left(\frac{u_0}{\nu L}\right)^{1/2} y, \quad w = \frac{u}{u_0}, \quad (11)$$

$$m = \frac{1}{(T_w - T_e)} \frac{d(T_w - T_e)}{d\xi}, \quad G = \frac{T_w - T}{T_w - T_e}, \quad \psi = (u_0 \nu L)^{1/2} f(\xi, \eta, \tau)$$

Equations (2) to (5) become

$$(b_1 f'')' + f''\theta + \frac{\partial w}{\partial \tau} + w \frac{\partial w}{\partial \xi} = \frac{\partial f'}{\partial \tau} + f' \frac{\partial f'}{\partial \xi} \quad (12)$$

$$(b_2 G')' + G'\theta + m(1 - G)f' = \frac{\partial G}{\partial \tau} + f' \frac{\partial G}{\partial \xi} \quad (13)$$

$$\eta = 0, \quad f = f' = 0, \quad G = 0 \quad (14a)$$

$$\eta = \eta_e, \quad f' = w, \quad G = 1 \quad (14b)$$

where

$$\theta = \frac{\partial f}{\partial \xi} \quad (15)$$

As we shall discuss in Section 3, the upstream conditions can be obtained by solving the above system with a special numerical solution provided that the

initial conditions are known. The latter can be obtained by making use of the steady-state conditions and expressing Eqs. (12) and (13) in the form

$$(b_1 f'')' + f''\theta + w \frac{\partial w}{\partial \xi} = f' \frac{\partial f'}{\partial \xi} \quad (16)$$

$$(b_2 G')' + G'\theta + m(1 - G)f' = f' \frac{\partial G}{\partial \xi} \quad (17)$$

There is no problem with the initial conditions for these equations since calculations are first performed for laminar flows which admit similarity solutions at the stagnation point. The transitional and/or turbulent flow calculations can then be started at any location away from the stagnation point by specifying the location of the onset of transition.

### 3.0 NUMERICAL METHOD

There are several numerical methods that can be used to solve the equations of the previous section, including the finite-difference methods due to Crank-Nicolson [29] and Keller [30]. Either scheme can be used satisfactorily for time-dependent boundary layers when there is no flow reversal across the layer although the Keller scheme has more desirable features than that of Crank-Nicolson for turbulent flows. When reversal occurs, and for problems associated with upstream boundary conditions such as those considered here, the advantages of the Keller scheme become more pronounced and necessitate its use as we shall discuss here. Only the solution of the continuity and momentum equations are discussed. The energy equation is linear and is uncoupled from the momentum equation so that its solution is straightforward and is described in detail in [27].

In this report the box scheme is used in two forms which depend upon the nature of the flow and, in particular on the presence or otherwise of reverse flow. The regular box scheme is used where the flow is always in the streamwise direction and is described in the following subsection. The characteristic box scheme, developed by Cebeci and Stewartson, is used to compute flows with negative streamwise velocities and also to generate the upstream boundary conditions discussed in subsection 2.2.

#### 3.1 Regular Box Scheme

To solve the momentum equation for steady-state conditions subject to its boundary conditions by Keller's scheme known as the Box method, we let  $f' = e$  and introduce a new function  $g$  defined by

$$e' = g \quad (18a)$$

and write Eqs. (15), (16) and (17) with  $b_1 = b$  as

$$\theta' = \frac{\partial e}{\partial \xi} \quad (18b)$$

$$(b_1 g)' + g\theta + w \frac{\partial w}{\partial \xi} = e \frac{\partial e}{\partial \xi} \quad (18c)$$

$$\eta = 0, \quad e = \theta = 0; \quad \eta = \eta_e, \quad e = w \quad (19)$$

To write the difference equations for the system given by Eqs. (18) and (19), we consider a net rectangle in which the net points are denoted by

$$\begin{aligned} \xi_0 &= 0, & \xi_i &= \xi_{i-1} + r_i, & r &= 1, 2, \dots, I \\ \eta_0 &= 0, & \eta_j &= \eta_{j-1} + h_j, & j &= 1, 2, \dots, J \end{aligned} \quad (20)$$

The finite-difference approximations to Eq. (18a) are obtained by averaging about the midpoint  $(\xi_i, \eta_{j-1/2})$ ,

$$h_j^{-1}(e_j^i - e_{j-1}^i) = g_{j-1/2}^i \equiv 1/2(g_j^i + g_{j-1}^i) \quad (21)$$

and those to Eqs. (18b,c) by centering all quantities except  $\theta$  at the center of the rectangle  $(\xi_{i-1/2}, \eta_{j-1/2})$  and taking the values of each say  $e$ , at the corners of the box, that is,

$$e_{j-1/2}^{i-1/2} = \frac{1}{2}(e_{j-1/2}^i + e_{j-1/2}^{i-1}) = \frac{1}{4}(e_j^i + e_{j-1}^i + e_j^{i-1} + e_{j-1}^{i-1}) \quad (22a)$$

The centering of  $\theta$  is achieved as

$$\theta_{j-1/2}^{i-1/2} = \frac{1}{2}(\theta_j^{i-1/2} + \theta_{j-1}^{i-1/2}) \equiv \frac{1}{2}(\theta_j + \theta_{j-1}) \quad (22b)$$

In this notation, the difference approximations to Eqs. (18b,c) can be written in the form:

$$h_j^{-1}(\theta_j - \theta_{j-1}) = r_i^{-1}(e_{j-1/2}^i - e_{j-1/2}^{i-1}) \quad (23a)$$

$$h_j^{-1}(b_j^i g_j^i - b_{j-1}^i g_{j-1}^i) + g_{j-1/2}^i \theta_{j-1/2} + g_{j-1/2}^{i-1} \theta_{j-1/2} - r_i^{-1}(e^2)_{j-1/2}^i = R_{j-1/2}^{i-1} \quad (23b)$$

where

$$R_{j-1/2}^{i-1} = - \{h_j^{-1}(b_j^{i-1} g_j^{i-1} - b_{j-1}^{i-1} g_{j-1}^{i-1}) - r_i^{-1}[(w^2)_{j-1/2}^i - (w^2)_{j-1/2}^{i-1} + (e^2)_{j-1/2}^{i-1}]\} \quad (24)$$

The boundary conditions, Eq. (19), become:

$$e_0 = \theta_0 = 0, \quad e_j = w_j \quad (25)$$

The system given by Eqs. (21), (23a,b) and (25) can be linearized by Newton's method and can be written as

$$\delta e_j - \delta e_{j-1} - \frac{h_j}{2}(\delta g_j + \delta g_{j-1}) = (r_1)_j \quad (26a)$$

$$\delta\theta_j - \delta\theta_{j-1} - \frac{1}{2} \left(\frac{h_j}{r_i}\right) (\delta e_j + \delta e_{j-1}) = (r_3)_{j-1} \quad (26b)$$

$$(s_1)_j \delta g_j + (s_2)_j \delta g_{j-1} + (s_3)_j \delta r_j + (s_4)_j \delta r_{j-1} + (s_5)_j \delta e_j + (s_6)_j \delta e_{j-1} = (r_2)_j \quad (26c)$$

$$\delta e_0 = \delta\theta_0 = 0, \quad \delta e_j = 0 \quad (27)$$

where

$$(r_1)_j = - (e_j^i - e_{j-1}^i) + h_j g_{j-1/2}^i \quad (28a)$$

$$(r_2)_j = R_{j-1/2}^{i-1} - [h_j^{-1} (b_j^i g_j^i - b_{j-1}^i g_{j-1}^i) + 2g_{j-1/2}^{i-1/2} \theta_{j-1/2} - r_i^{-1} (e^2)_j^i] \quad (28b)$$

$$(r_3)_{j-1} = - (\theta_j - \theta_{j-1}) + \frac{h_j}{r_i} (e_{j-1/2}^i - e_{j-1/2}^{i-1}) \quad (28c)$$

$$(s_1)_j = b_j h_j^{-1} + \frac{1}{2} \theta_{j-1/2} \quad (s_3)_j = g_{j-1/2}^{i-1/2} \quad (s_5)_j = -r_i^{-1} e_j \quad (29)$$

$$(s_2)_j = -b_{j-1} h_j^{-1} + \frac{1}{2} \theta_{j-1/2} \quad (s_4)_j = (s_3)_j \quad (s_6)_j = -r_i^{-1} e_{j-1}$$

The resulting linear system, Eqs. (26) and (27), can be written in the form

$$\underline{A} \underline{\delta}_j = \underline{r}_j \quad (30)$$

and can be solved by the 3 x 3 algorithm based on the block elimination method described in [27].

### 3.2 Characteristic Box Scheme

The procedure of the previous sub-section provides a solution of Eq. (16), starting at the stagnation point  $\xi = \xi_S$ , for a prescribed velocity distribution  $w(\xi)$  at  $\tau(0) = 0$  and, as a result, the solutions on the next time "line" can be determined by an explicit method. If we wish to avoid stability problems, however, an implicit method is required and the generation of upstream boundary conditions for the momentum equation (and the energy equation) becomes more difficult. An accurate and efficient method for this purpose is the characteristic box scheme which is able to deal with the moving stagnation point and the flow reversals which result.

To describe the characteristic box scheme, we note the definition of local streamlines and write

$$d\tau = \frac{d\xi}{e} \quad (31)$$

If we designate distance in this direction by  $s$  and the angle that it makes with the  $\tau$ -axis by  $\beta$ , (see Fig. 4) then Eq. (18c), which in terms of new variables  $e$  and  $g$ , is

$$(bg)' + g\theta + \frac{\partial w}{\partial \tau} + w \frac{\partial w}{\partial \xi} = \frac{\partial e}{\partial \tau} + e \frac{\partial e}{\partial \xi} \quad (32)$$

can be written as

$$(bg)' + g\theta + \frac{\partial w}{\partial \tau} + w \frac{\partial w}{\partial \xi} = \lambda \frac{\partial e}{\partial s} \quad (33)$$

where

$$\lambda = \sqrt{1 + e^2} \quad (34a)$$

$$\beta = \tan^{-1} e \quad (34b)$$

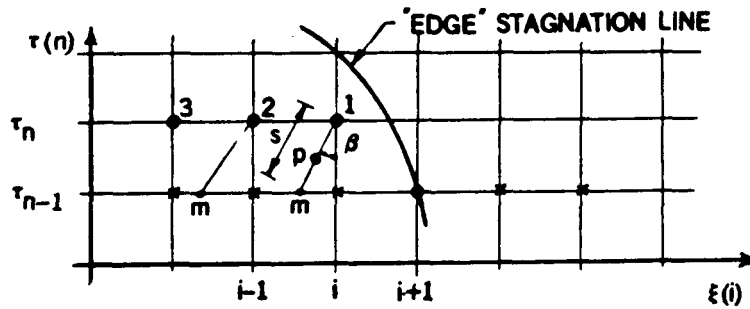


Figure 4. Notation and grid for the Characteristic Box scheme. For details, see [25].

The solution procedure for the system given by Eqs. (15a,b), (16) and (33) is similar to that of the previous sub-section with small differences due to the manner in which the difference equations are written for Eq. (33). Also, since now we are considering a three-dimensional form of the equation, we also consider the net points

$$\tau_0 = 0, \quad \tau_n = \tau_{n-1} + k_n \quad n = 1, 2, \dots, N \quad (35)$$

in addition to those given by Eq. (20). The difference approximations to Eqs. (18a,b) are identical to those given by Eq. (21), (23a) except that the superscripts  $i$  on each variable also include  $n$ . To obtain the solutions on the first time line  $\tau_1$ , let us assume that the stagnation line based on the external streamline is given, the solution of point 1 is known, and direct our attention to point 2. The finite-difference approximations to Eq. (33) are written along the streamline direction (see Fig. 4) at point P

$$\begin{aligned}
& \frac{h_j^{-1}}{2} (b_j^{i,n} g_j^{i,n} - b_{j-1}^{i,n} g_{j-1}^{i,n}) + \frac{h_j^{-1}}{2} (b_j^{m,n-1} g_j^{m,n-1} - b_{j-1}^{m,n-1} g_{j-1}^{m,n-1}) \\
& + \frac{1}{2} (g_{j-1/2}^{i,n} + g_{j-1/2}^{m,n-1}) \theta_{j-1/2}^P + \frac{\partial w}{\partial \tau} (P) + w \frac{\partial w}{\partial \xi} (P) \\
& = \frac{1}{2} (\lambda_{j-1/2}^{i,n} + \lambda_{j-1/2}^{m,n-1}) \frac{e_{j-1/2}^{i,n} - e_{j-1/2}^{m,n-1}}{\Delta s_{j-1/2}}
\end{aligned} \tag{36}$$

where

$$\Delta s_{j-1/2} = \frac{k_n}{\cos \beta_{j-1/2}} \tag{37}$$

The relation between  $\theta_{j-1/2}^P$  and those values of  $\theta$  centered at  $(i-1/2, n-1/2)$  and  $(i-3/2, n-1/2)$  are

$$\theta_{j-1/2}^P = \frac{\theta_{j-1/2}^{i-3/2} - \theta_{j-1/2}^{i-1/2}}{\xi_{i-3/2} - \xi_{i-1/2}} (\xi^P - \xi_{i-3/2}) + \theta_{j-1/2}^{i-3/2} \tag{38}$$

Rearranging Eq. (36) and denoting  $R_{j-1/2}^{m,n-1}$  by

$$\begin{aligned}
R_{j-1/2}^{m,n-1} = & - [h_j^{-1} (b_j^{m,n-1} g_j^{m,n-1} - b_{j-1}^{m,n-1} g_{j-1}^{m,n-1}) + 2 \frac{\partial w}{\partial \tau} (P) + 2(w \frac{\partial w}{\partial \xi})(P) \\
& + \lambda_{j-1/2}^{m,n-1} \frac{e_{j-1/2}^{m,n-1}}{\Delta s_{j-1/2}} ]
\end{aligned} \tag{39}$$

it can be shown that the linearized version of the resulting expression can be expressed in the same form as Eq. (26c), with

$$(s_1)_j = h_j^{-1} + c_7 \qquad (s_2)_j = -h_j^{-1} + c_7 \tag{40}$$

$$(s_3)_j = (s_4)_j = -\frac{c_1}{2} (g_{j-1/2}^{i,n} + g_{j-1/2}^{m,n-1})$$

$$(s_5)_j = -c_4 + \frac{c_6}{\lambda_{j-1/2}^{i,n}} e_j \quad (s_6)_j = -c_5 + \frac{c_6}{\lambda_{j-1/2}^{i,n}} e_{j-1}$$

and

$$(r_2)_j = R_{j-1/2}^{m,n-1} - [h_j^{-1} (b_j^{i,n} g_j^{i,n} - b_{j-1}^{i,n} g_{j-1}^{i,n}) + (g_{j-1/2}^{i,n} + g_{j-1/2}^{m,n-1}) \theta_{j-1/2}^P - (\lambda_{j-1/2}^{i,n} + \lambda_{j-1/2}^{m,n-1}) \frac{e_{j-1/2}^{i,n}}{\Delta s_{j-1/2}} - \lambda_{j-1/2}^{i,n} \frac{e_{j-1/2}^{m,n-1}}{\Delta s_{j-1/2}}] \quad (41)$$

where  $c_1$  to  $c_7$  are given by

$$c_1 = \frac{\xi^D - \xi_{i-3/2}}{\xi_{i-3/2} - \xi_{i-1/2}}, \quad c_2 = r_{j-1/2}^{i-3/2}, \quad c_3 = \frac{1}{\Delta s_{j-1/2}}$$

$$c_4 = \frac{c_3}{2} \left[ \frac{e_j^{i,n}}{\lambda_{j-1/2}^{i,n}} e_{j-1/2}^{i,n} + \lambda_{j-1/2}^{i,n} + \lambda_{j-1/2}^{m,n-1} \right],$$

(42)

$$c_5 = \frac{c_3}{2} \left[ \frac{e_{j-1}^{i,n}}{\lambda_{j-1/2}^{i,n}} e_{j-1/2}^{i,n} + \lambda_{j-1/2}^{i,n} + \lambda_{j-1/2}^{m,n-1} \right],$$

$$c_6 = \frac{c_3}{2} e_{j-1/2}^{m,n-1}, \quad c_7 = \frac{1}{2} [c_1 (c_2 - \theta_{j-1/2}^{i-1/2}) + c_2]$$

The resulting equation, which is analogous to Eq. (23c) can then be solved together with Eqs. (23a,b) and (24) by using the same block-elimination method employed to solve the system given by Eqs. (23) and (24).

To generate the upstream boundary conditions, let us initially assume that the first profile on either side of the "edge" stagnation point is known and that we are interested in computing the flow say at 2 (see Fig. 4). If there is now flow reversal at that point, then an extension of the procedure discussed in the previous sub-section can be used to obtain a solution there. In the presence of flow reversal, we use the characteristic box scheme on an iterative basis. To explain this further, let us assume that  $\theta_j$  in Eq. (36) is known, then the solution of the momentum equation at point 1 by the characteristic method can be achieved by solving Eqs. (23a,c) in the form

$$\delta e_j - \delta e_{j-1} - \frac{h_j}{2} (\delta g_j + \delta g_{j-1}) = (r_1)_j \quad (43a)$$

$$(s_1)_j \delta g_j + (s_2)_j \delta g_{j-1} + (s_5)_j \delta e_j + (s_6)_j \delta e_{j-1} = (r_2)_j \quad (43b)$$

subject to the boundary conditions

$$\delta e_0 = 0, \quad \delta e_j = 0 \quad (44)$$

Once a solution for the point 1 is known, solutions to all the points to the right and to the left of point 1 can be obtained by the general characteristic scheme without further approximations. Thus the only approximation on a given time line results from the solutions generated at point 1. Our calculations have shown that the influence of point 1 on its neighbors decreases with distance. Thus the approximate solution at point 1 can be further improved by repeating the calculations at point 1.

## 4.0 RESULTS AND DISCUSSION

The numerical procedures of the previous section have been used to obtain solutions of the continuity, momentum and energy equation for three model problems. The results are presented and discussed in the following three subsections and correspond to uniform wall temperature ( $m = 0$ ) and Prandtl number 0.72. The first two model problems involve laminar flows and the third addresses laminar and turbulent flows. It should be emphasized that these model problems have been designed to test the numerical procedure which has been formulated in a general way so that its application can readily be extended to the more practical flows discussed in the introduction.

In regions where there was no flow reversal, the standard box scheme has been used. Where the calculations revealed flow reversal, the solution procedure subsequently made use of the characteristic box scheme.

### 4.1 Oscillating Airfoil Model

The first model problem corresponds to flow over an ellipse with a thickness ratio  $\gamma (\equiv b/a)$  and with  $\gamma \ll 1$  at an angle of  $\alpha$ . The surface of the body is defined by

$$\bar{x} = -a \cos\phi, \quad \bar{y} = a\gamma \sin\phi, \quad -\pi < \phi < \pi \quad (45)$$

With these definitions and to a first-order approximation, the external velocity for the steady flow in the leading of a thin ellipse can be deduced from inviscid flow theory to be

$$\bar{u}_e(z) = \frac{z + z_0}{\sqrt{1 + z^2}} \quad (46)$$

Here  $\bar{u}_e(z)$  denotes a dimensionless velocity, the parameter  $z$  denotes a dimensionless distance related to the  $\bar{x}$ - and  $\bar{y}$ -coordinates of the ellipse by  $\bar{x} + a = (1/2)a\gamma^2 z^2$ ,  $\bar{y} = a\gamma^2 z$  measured from the nose, and  $z_0$  represents a reduced angle of attack. The parameter  $z$  is also related to the dimensionless surface distance  $\xi$  with  $L = \gamma^2 a$  by  $\xi = \int_0^z (1 + z^2)^{1/2} dz$ . In the present study we extend Eq. (46) to unsteady flows by introducing time dependency as

$$\bar{u}_e(z, \tau) = \frac{z + z_0(1 + c \sin\omega\tau)}{\sqrt{1 + z^2}} \quad (47)$$

Figures 5 to 8 show the calculated results for two circular frequencies,  $\omega = \pi/30, \pi/3$  with  $z_0 = 1$  and  $c = -1/2$ . They demonstrate the effects of the frequency on the wall shear  $f''(0)$ , wall heat flux  $G'(0)$  and dimensionless displacement thickness,  $\Delta^*$ , which are defined by

$$f''(0) = \frac{\tau_w}{\rho u_0^2} \sqrt{R_L} \quad , \quad G'(0) = \frac{\dot{q}_w L}{k \sqrt{R_L} (T_w - T_e)} \quad (48a)$$

$$\Delta^* = \frac{1}{L} \frac{u_e}{u_0} \sqrt{R_L} \int_0^\infty \left(1 - \frac{u}{u_e}\right) dy \quad (48b)$$

The results of Figures 5a and 5b indicate that the time dependent effects on the solutions increase significantly as the circular frequency  $\omega$  changes from  $\omega = \pi/30$  to  $\pi/3$ . While the wall shear and displacement thickness values computed at  $\omega\tau = \pi$  and  $2\pi$  with  $\omega = \pi/30$  are nearly the same as those at  $\tau = 0$ , they differ considerably from each other when  $\omega = \pi/3$ . The results in Figure 6 show, however, that increasing the circular frequency by a factor of ten has practically no effect on the wall heat flux.

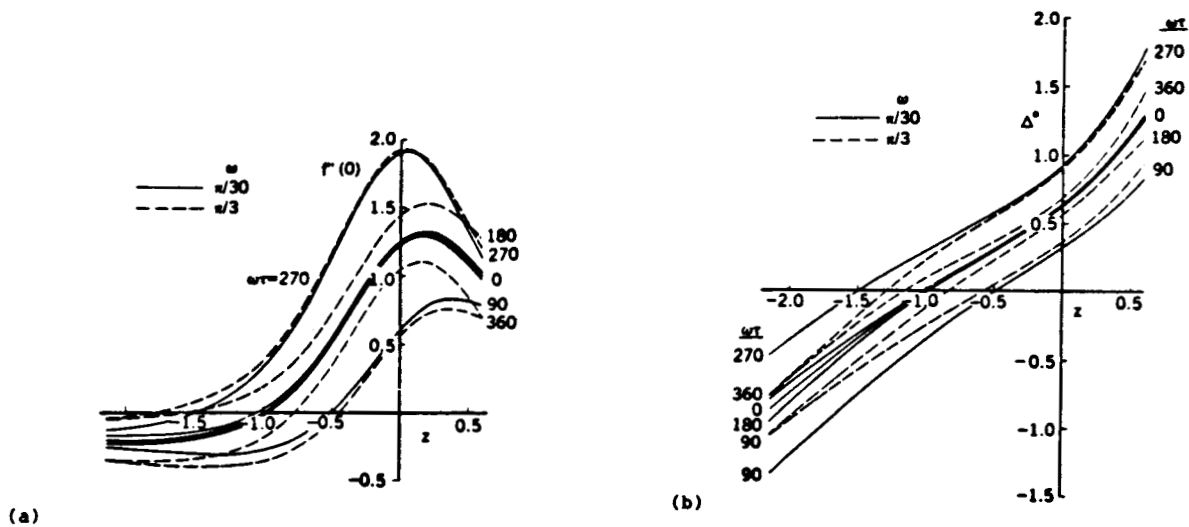


Figure 5. The effect of frequency on the (a) wall shear parameter,  $f'(0)$ , (b) displacement thicknesses,  $\Delta^*$ , of the first model problem.

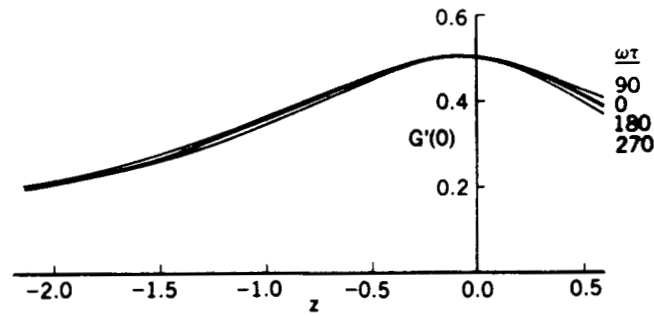


Figure 6. Variation of the wall heat flux parameter,  $G'(0)$ , with  $z$  for the first model problem with  $\omega = \pi/30$ . The results with  $\omega = \pi/3$  are virtually identical to those obtained with the smaller frequency.

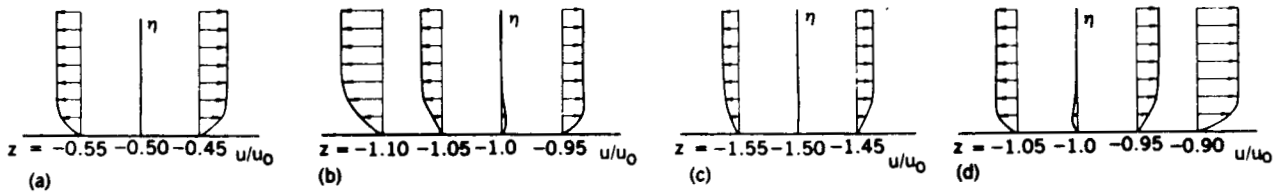


Figure 7. Variation of the velocity profiles for  $\omega = \pi/30$  near the stagnation region of the first model problem for different values of  $\omega\tau$ , (a) 90, (b) 180, (c) 270, (d) 360.

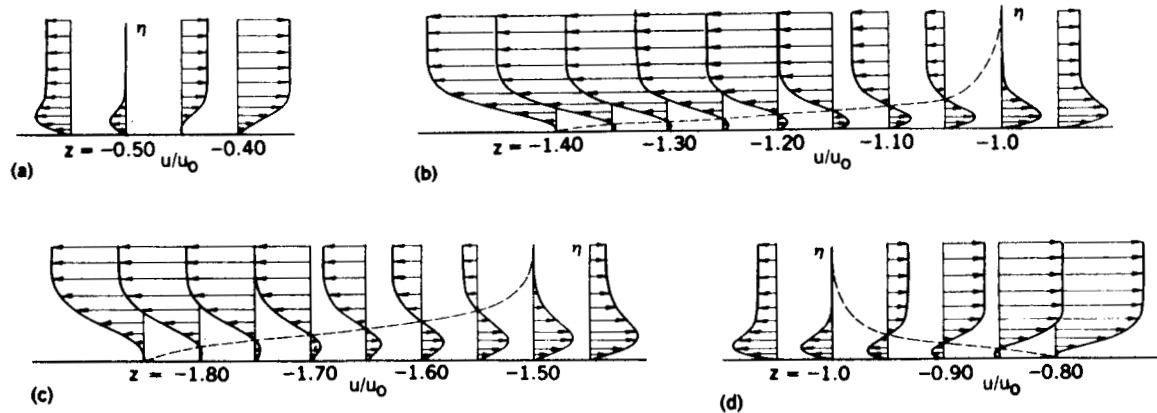


Figure 8. Variation of the velocity profiles for  $\omega = \pi/3$  near the stagnation region of the first model problem for different values of  $\omega\tau$ , (a) 90, (b) 180, (c) 270, (d) 360. The dashed line indicates the locus of zero  $u$ -velocity.

Figures 7 and 8 allow the examination of the effect the frequency has on the calculated velocity profiles in the vicinity of the stagnation point. Figure 7 shows that the locus of the  $u$ -velocity on time lines  $\tau = \pi/2$  and  $\pi$  is

essentially the same as in the steady case and as a result there are no flow reversals in the velocity profiles. However, as can be seen from Figure 8, increasing the frequency to  $\pi/3$ , flow reversals begin to occur around the stagnation point and become rather prolonged as time increases to  $\omega\tau = 3\pi/2$ . At  $\omega\tau = 2\pi$ , the region of flow reversal is reduced but is not zero, as it was at  $\omega\tau = 0$ .

#### 4.2 Gust Response Model

The second model problem allows us to study the transient motion between the two steady stagnation flows similar to those an airfoil would encounter during a gust or change in incidence as an initially steady-flow accelerates from  $u_e/u_\infty = \xi$  to  $u_e/u_\infty = 2(\xi - 1)$ . For this purpose we use Eq. (1) with  $\omega = \pi/8$  and

$$A(\tau) = 2 - \cos^2\omega\tau, \quad B(\tau) = \sin^2\omega\tau \quad 0 \leq \tau \leq 8 \quad (49)$$

This flow has been studied by Cebeci, Stewartson and Williams [28] with slightly different forms of  $A(\tau)$  and  $B(\tau)$

$$A(\tau) = 2 - e^{-\tau}, \quad B(\tau) = 1 - e^{-\tau} \quad (50)$$

than those used here. Our modified expressions were required to ensure that  $(\partial u_e/\partial t)$  is equal to zero at  $t = 0$ , as discussed previously.

Figure 9 shows a comparison between the two external velocities considered in [28] and in the present study, and Figure 10 shows the results of the present

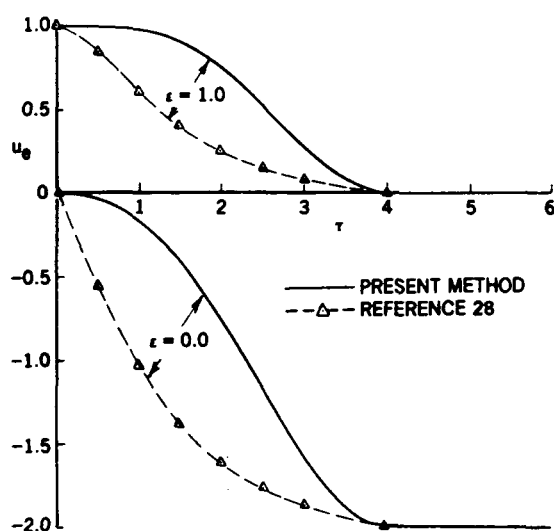


Figure 9. Variation of external velocity with time for the second model problem.

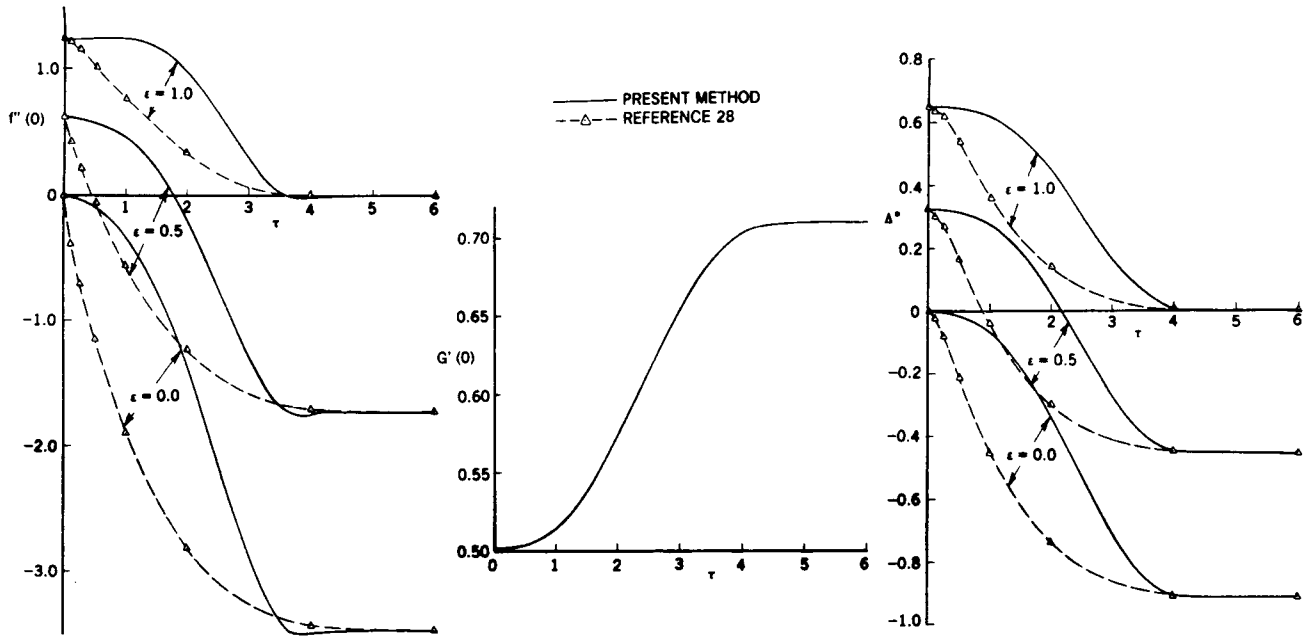


Figure 10. Variation with time of (a) wall shear parameter,  $f''(0)$ , (b) wall heat flux parameter,  $G'(0)$ , and (c) displacement thickness,  $\Delta^*$  for the second model problem.

calculations together with those of [28]. Our calculated results correspond to nondimensional forms of the wall shear,  $f''(0)$ , wall heat flux,  $G'(0)$ , and displacement thickness,  $\Delta^*(\equiv \sqrt{R_L} \delta_0^*/L)$  where

$$\delta_0^* = \frac{1}{u_0} \int_0^{\infty} (u_e - u) dy \quad (51)$$

The results of [28] were obtained for momentum based properties which are linked to the above definitions by

$$f''(0) = (\xi - B)\tau + g''(0) \quad (52)$$

$$\Delta^* = (\xi - B)\delta_0^* - g_{\infty} \quad (53)$$

with  $\tau$ ,  $g''(0)$ ,  $\delta_0^*$  and  $g_{\infty}$  denoting here the parameters computed in [28].

As expected, the results in Figures 10a and 10c show that the behavior of  $f''(0)$  and  $\Delta^*$  is different during the transient motion due to the use of different functions for  $A(\tau)$  and  $B(\tau)$ . In each case, however, the solutions approach the asymptotic values relatively fast. The results for  $G'(0)$ , shown in Fig. 10b, were obtained with the present method since the study of [28] did not

consider the energy equation. Again, as expected, the solutions of the energy equation approach the asymptotic value of 0.7095 [27].

#### 4.3 Rotor Wake Model

The third model problem involves flow on a circular cylinder of diameter  $D$  which experiences the periodic passing of wakes. It corresponds to the experimental arrangement of [20], see Fig. 2, and permits comparison between calculations performed for turbulent flows with measurements. The model problem is first addressed in terms of laminar flow to test the numerical procedure.

Figure 11 shows the flow configuration and the notation for this model problem. For a time period  $t_g$ , the cylinder is subjected to a freestream velocity  $V_\infty$  and for  $t_w$  it is immersed in a superimposed rotating wake which has a rotational component  $\omega r$ . The cycle repeats itself with a blade passing frequency  $F(\equiv 1/(t_g + t_w))$  and is related to the Strouhal number  $St$  by  $FD/V_\infty$ . To derive dimensionless expressions for the parameters  $A(\xi, \tau)$  and  $B(\tau)$  in Eq. (1) needed to define the external velocity distribution near the stagnation region, we adopt the procedure discussed in the Appendix.

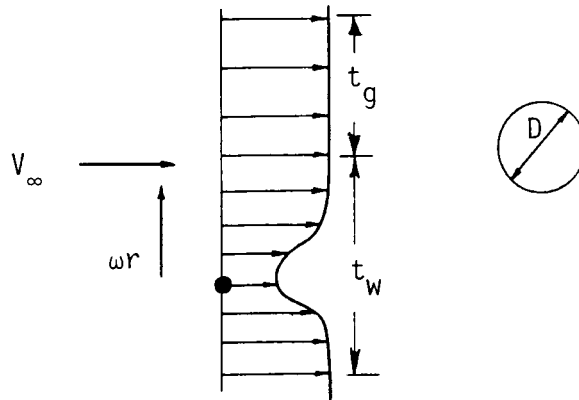


Figure 11. Notation and flow configuration for the rotor-wake model.

At first the calculations were performed for a laminar flow in order to test the numerical procedure. With the choice of  $E_2 = \sqrt{10}$ ,  $E_1 = 100$  and  $V_m = 1/3$ , the parameters  $A$ ,  $B$  and  $f$ , Eqs. (A-15) to (A-17) become

$$A(\tau) = [f^2 + 10(St)^2(1 - f)^2]^{1/2} \quad (54)$$

$$B(\tau) = \tan^{-1} \left[ \sqrt{10} \text{St} \left( \frac{1-f}{f} \right) \right] \quad (55)$$

$$f = \frac{2}{3} + \frac{1}{3} \cos[\pi(1 - 100 \text{St}\tau)] \quad (56)$$

The computed values of wall heat flux,  $G'(0)$  for two values of Strouhal number show that they are not influenced by the changes in the freestream velocity and are virtually constant for the range of  $\xi$  and  $\tau$  values considered with  $G'(0) \sim 0.50$  for  $\text{St} = 0.1$  and  $G'(0) \sim 0.51$  for  $\text{St} = 0.2$ . On the other hand, as shown in Fig. 13, the computed values of wall shear,  $f''(0)$ , for  $\text{St} = 0.1$  are significantly influenced by the changes in the freestream velocity which causes flow reversals in the velocity profiles around the stagnation point based on the vanishing of the external velocity. The movement of the stagnation point and the resulting flow reversals increase with time and with space. For example, the calculations for steady state have the stagnation point at  $\xi = 0$ , and, as expected, there is no flow reversal on either side of the stagnation point. At  $\tau = 0.05$ , the stagnation point moves to  $\xi = 0.15$  but the flow reversals in the velocity profiles continue up to and including  $\xi = 0.85$  as can be seen from the results shown in Fig. 14. At  $\tau = 0.10$ , Fig. 13, the stagnation point has moved to  $\xi = 0.55$  but the flow reversals persist for a longer distance and continue until  $\xi = 1.20$ . As can be seen from the velocity profiles in Fig.

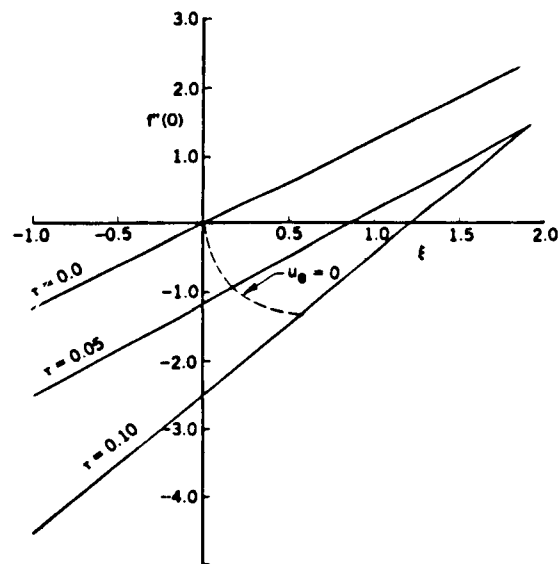


Figure 13. Variation of the wall shear parameter,  $f''(0)$ , with  $\xi$  for the third model problem.  $\text{St} = 0.10$ .

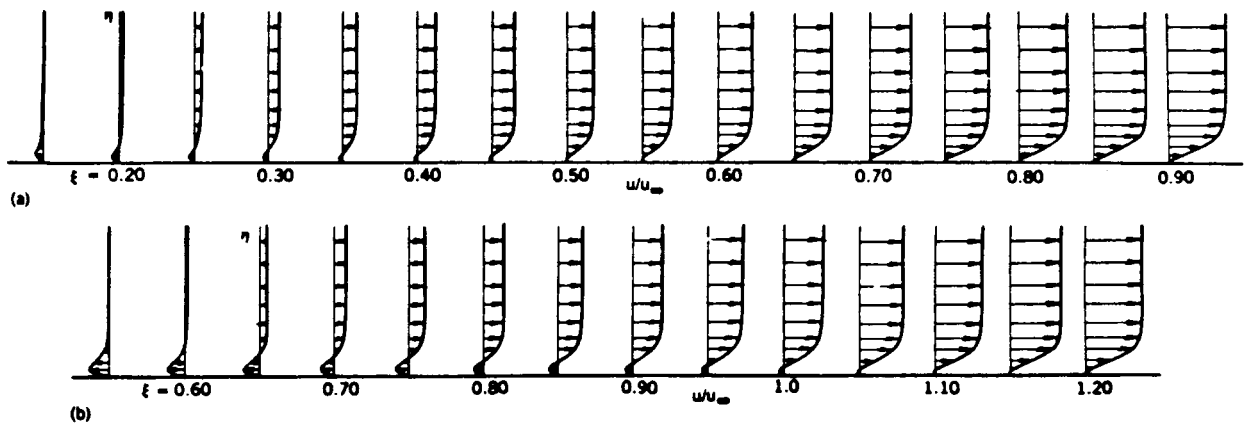


Figure 14. Variation of the velocity profiles near the stagnation region of the third model problem for two values of time. (a)  $\tau = 0.05$ , (b)  $\tau = 0.10$ .

14, the region of flow reversal across the layer has now increased and is substantially more pronounced than that at  $\tau = 0.05$ .

The wall shear and displacement thickness results for  $St = 0.2$  show similar trends. As expected, the flow reversals in the velocity profiles, for example at  $\tau = 0.10$ , are bigger than those at  $St = 0.1$  but cover the same range in  $\xi$ .

The above laminar flow results show that the numerical procedure is able to obtain solutions for a range of blade-passing frequencies of practical relevance. The movement of the stagnation point with space and time and the resulting flow reversals around the stagnation point cause no computational difficulties and the numerical tests show that the accuracy is better than required for practical problems.

The present method is applicable to laminar, transitional and turbulent flows. It requires that the calculations start as laminar from the stagnation point. The onset of transition can be assigned to occur in accordance with experiments and the subsequent transitional and turbulent flows can be represented by the algebraic eddy-viscosity model described in Section 2.2. As a consequence of this model, the length of the transitional region is depended upon the free-stream conditions.

In the case of turbulent flow, estimates of  $E_1$ ,  $E_2$  and  $V_m$  can be obtained from the experiments of Ref. 20. We note that  $D$  represents the diameter of the

heated stator,  $d$  the diameter of the rotating pin,  $S$  the separation distance between the two pins of diameter  $d$  and  $D$  (see Fig. 2),  $r$  the distance from the axis of rotation,  $C_D$  the drag coefficient of the  $n$  number of rotating pins, and  $V_m$  the wake centerline velocity. The experimental values are  $D = 12.7\text{mm}$ ,  $d = 3.18\text{mm}$ ,  $S = 25.4\text{mm}$ ,  $r = 16.925\text{cm}$ ,  $C_D = 1.2$ ,  $n = 24$ ,  $V_m = 0.62$ , so that  $E_1 = 79$ ,  $E_2 = 3.49$  and

$$A(\tau) = [f^2 + (3.49)^2(St)^2(1 - f^2)]^{1/2} \quad (57)$$

$$B(\tau) = \tan^{-1} [3.49 (\frac{1-f}{f})] \quad (58)$$

$$f = 0.81 + 0.19 \cos[\pi(1 - 79 St\tau)] \quad (59)$$

Calculations using Eqs. (57) to (59) in Eq. (1) were performed in the above manner to simulate the near stagnation region of the flow of [20]. The onset of transition was set very close to the stagnation point and transitional and turbulent flow calculations were performed for  $0 \leq t \leq t_w + t_g$ , for one cycle for the experimental Reynolds number of  $R_d = 76,000$ . Since the experimental data suggests that the average Nusselt number is relatively constant and is ten-percent higher than that of laminar flow, it was assumed that the transitional region was negligibly short. Furthermore, the present eddy-viscosity model is a function of the velocity field and the heat transfer parameter is relatively constant in the stagnation region  $0 \leq \theta \leq 40^\circ$ , so that it was further assumed that the eddy viscosity in this region be constant. This implies that the distribution of eddy viscosity determined at the end of the transitional region [ $\gamma_{tr} = 1$ ] retains the same numerical value throughout the turbulent flow calculations. As a consequence of the above, the ratios of the average Nusselt number,  $Nu$ , on the blade passing a wake to that of a blade in a freestream during one cycle,  $Nu_s$ , used in the presentation of the experimental results were calculated from

$$\frac{Nu}{Nu_s} = \frac{Nu_b + Nu_g}{Nu_s} = \frac{\int_0^{t_w} Nu dt + \int_{t_w}^{t_w+t_g} Nu dt}{\int_0^{t_w+t_g} Nu dt} \quad (60)$$

Since the cycle time is  $t_w + t_g$ , the numerator of Eq. (60) contains two parts, one for the blade being submerged in the wake,  $Nu_b$ , and the other for the base in a freestream,  $Nu_g$ , during time  $t_g$  where the flow is laminar and admits

similarity. In the transformed coordinates of the calculations, the ratio of the averaged Nusselt number may be written as

$$\frac{Nu}{Nu_s} = \frac{\int_0^{2\pi} G'_w d\tau + (G'_w)_l t_g}{(G'_w)_l (t_g + t_w)} \quad (61)$$

where  $(G'_w)_l = 1.0034$  for laminar flows. The measured and calculated values of average Nusselt number ratios were found to be 1.1 and 1.09, respectively, and constant throughout the turbulent flow region. The closeness of the two results is gratifying but should be viewed with caution bearing in mind the assumptions which have been made in relation to the eddy-viscosity model and the assumed freestream velocity distribution. Alternative approaches to the representation of the turbulence characteristics of the stagnation region have been examined, for example by Taulbee and Tran [31], and deserve future consideration. In addition, the integration of the heat transfer parameter  $G'_w$  is subject to some uncertainty in the blending region between laminar and turbulent flows.

## 5.0 CONCLUDING REMARKS

The work of the preceding sections represents essential steps in the development of a general method for the calculation of unsteady heat transfer on turbine blades. It has emphasized the stagnation region since this must be correctly represented in order for the method to calculate the flow and heat-transfer characteristics of a blade passage. This region involves a moving stagnation point with consequent reverse flows and has required the development and use of a novel numerical procedure to solve the equations for conservation of mass, momentum and energy. The characteristic box scheme, with its stability requirements, has been used in regions of reverse flow and the standard box scheme elsewhere. Transitional and turbulent flow have been represented by an eddy-viscosity formula.

The method has been applied to three model problems devised to allow its quantitative evaluation. They correspond to an ellipse, with leading-edge geometry similar to that of a thin airfoil, oscillating with a uniform-velocity onset flow; a stationary airfoil subjected to an onset velocity which changes suddenly; and to a cylinder which experiences an onset flow with periodic wakes. Laminar-flow calculations were performed for these three model flows and results presented to demonstrate that the method is able to calculate their essential features in a convenient and numerically accurate manner. The third problem simulates an experimental arrangement for which heat-transfer measurements have been reported and calculations were performed to include the transitional- and turbulent-flow regions; again the method predicted results which represented the essential features of the flow, including an averaged Nusselt number in close agreement with the measured value.

The results confirm that the calculation method correctly predicts the flow characteristics of the stagnation region of unsteady flows of relevance to blades subjected to onset velocities which vary in space and in time. The method can now be extended to include procedures for the solution of the unsteady, inviscid-flow equations and to ensure interaction between the inviscid and boundary-layer flows. Both procedures have already been developed so that the general method can be assembled and applied to blade-passage flows.

## 6.0 REFERENCES

1. Dennis, A. and Cruse, T.: Cost Benefits from Improved Hot Section Life Prediction Technology. AIAA Paper 79-1154, June 1979.
2. Dankoff, W., Herr, P. and McIlwain, M.C.: Space Shuttle Main Engine (SSME) - The Maturing Process. Aero & Astro. Vol. 21, No. 1, pp. 26-32, 1983.
3. Sokolowski, D.E. and Ensign, C.R.: Improved Durability in Advanced Combustors and Turbines Through Enhanced Analytical Design Capabilities. AIAA Paper 85-1417, July 1985.
4. Sokolowski, D.E. and Ensign, C.R.: Toward Improved Advanced Combustors and Turbines - Progress in the Prediction of Thermomechanical Loads. ASME Paper 86-6T-172, June 1986.
5. Marsik, S.J. (ed): Structural Integrity and Durability of Reusable Space Propulsion Systems. NASA CP-2381, June 1985.
6. Stepka, F.S.: Analysis of Uncertainties in Turbine Metal Temperature Predictions. NASA TP-1593, 1980.
7. Rudey, R.A. and Graham, R.W.: A Review of NASA Combustor and Turbine Heat Transfer Research. NASA TM-83541, 1984.
8. Suo, M.: Turbine Cooling. In Aerothermodynamics of Aircraft Gas Turbine Engines (G.C. Oates, ed.), Chap. 19, AFAPL-TR-78-52, July 1978.
9. Metzger, D.E. and Mayle, R.E.: Heat Transfer: Gas Turbine Engines. Mech. Eng., Vol. 105, No. 6, pp. 44-52, 1983.
10. Simoneau, R.J.: Heat Transfer in Aeropropulsion Systems. Proceedings of the 1985 U.S.-Japan Heat Transfer Joint Seminar. San Diego, Sept. 1985 (NASA TM 87066).

11. Dring, R.P., Joslyn, H.D., Hardin, L.W. and Wagner, J.H.: Turbine Rotor-Stator Interaction. J. Eng. for Power, Vol. 104, No. 4, pp. 729-742, 1982.
12. Sharma, O.P., Butler, T.L., Joslyn, H.D. and Dring, R.P.: An Experimental Investigation of the Three-Dimensional Unsteady Flow in an Axial Flow Turbine. AIAA Paper 83-1170, June 1983.
13. Hodson, H.P.: Measurements of Wake-Generated Unsteadiness in the Rotor Passages of Axial Flow Turbines. J. Eng. for Gas Turbines and Power, Vol. 7, No. 2, pp. 467-476, 1985.
14. Binder, A., Forster, W., Kruse, H. and Rogge, H.: An Experimental Investigation into the Effect of Wakes on the Unsteady Turbine Rotor Flow. J. Eng. for Gas Turbines and Power, Vol. 7, No. 2, pp. 458-466, 1985.
15. Dunn, M.G.: Heat-flux Measurements for the Rotor of a Full-Stage Turbine: Part I, Time-Averaged Results. ASME Paper 86-GT-77, June 1986.
16. Dunn, M.G., George, W.K., Rae, W.J., Moller, J.C., Woodward, S.H. and Seymour, P.J.: Heat-Flux Measurements for the Rotor of a Full-Stage Turbine: Part II, Description of Analysis Technique and Typical Time Resolved Measurements. ASME Paper 86-GT-78, June 1986.
17. Doorly, D.J. and Oldfield, M.L.G.: Simulation of the Effects of Shock Wave Passing on a Turbine Rotor Blade. J. Eng. for Gas Turbines and Power, Vol. 107, No. 4, pp. 998-1006, Oct. 1985.
18. Ashworth, D.A., LaGraff, J.E., Schultz, D.L. and Grinrod, K.J.: Unsteady Aerodynamic and Heat Transfer Processes in a Transonic Turbine Stage. J. Eng. for Gas Turbines and Power, Vol. 107, No. 4, pp. 1011-1030, Oct. 1985.

19. O'Brien, J.E., Simoneau, R.J., LaGraff, J.E. and Morehouse, K.A.: Unsteady Heat Transfer and Direct Comparison to Steady-State Measurements in a Rotor-Wake Experiment. Proceedings of the 8th Inter. Heat Transfer Conf., Aug. 1986. (NASA TM 87220).
20. Morehouse, K.A. and Simoneau, R.J.: Effect of a Rotor Wake on the Local Heat Transfer on the Forward Half of a Circular Cylinder. Proceedings of the 8th Inter. Heat Transfer Conf., Aug. 1986. (NASA TM 87234).
21. Shamroth, S.J.: A Turbulent Flow Navier-Stokes Analysis for an Airfoil Oscillating in Pitch. In Unsteady Turbulent Shear Flows (R. Michel, J. Cousteix and R. Houdeville, eds.) pp. 185-190, Springer, 1981.
22. Rai, M.M.: Navier-Stokes Simulations of Rotor-Stator Interaction Using Patched and Overlaid Grids. AIAA Paper 85-1519, July 1985.
23. Cebeci, T., Stewartson, K. and Williams, P.G.: Separation and Reattachment Near the Leading Edge of a Thin Airfoil at Incidence. AGARD CP 291, Paper 20, 1981.
24. Cebeci, T., Clark, R.W., Chang, K.C., Halsey, N.D. and Lee, K.: Airfoils with Separation and the Resulting Wakes. J. Fluid Mech. 163, 323, 1986.
25. Cebeci, T., Carr, L.W., Khattab, A.A. and Schimke, S.M.: Computational Aspects of Unsteady Flows. AGARD, CPP 386, France, May 1985.
26. Cebeci, T., Khattab, A.A. and Schimke, S.M.: Separation and Reattachment Near the Leading edge of a Thin Oscillating Airfoil. J. Fluid Mech. 188, pp. 253-274, 1988.
27. Cebeci, T. and Bradshaw, P.: Physical and Computational Aspects of Convective Heat Transfer. Springer-Verlag, N.Y., 1984.
28. Cebeci, T., Stewartson, K. and Williams, P.G.: On the Response of a Stagnation Boundary Layer to a Change in the External Velocity. SIAM J. Appl. Math., Vol. 36, pp. 190-199, 1979.

29. Crank, J. and Nicolson, P.: A Practical Method of Numerical Evaluation of Solutions of Partial-Differential Equations of the Heat Conduction Type. Proc. Cambridge Phil. Soc. 43, p. 50, 1947.
30. Keller, H.B., Numerical Methods in Boundary-Layer Theory. Ann. Rev. Fluid Mech. Vol. 10, pp. 417-433, 1978.
31. Taulbee, D.B. and Tran, L.: Stagnation Streamline Turbulence. To be published in the AIAA J.

Appendix  
EXTERNAL VELOCITY DISTRIBUTION IN THE STAGNATION REGION  
WITH NONUNIFORM ONSET FLOW

Consider a fixed circular cylinder of diameter  $D$  in a uniform flowfield  $V_\infty$  which is disturbed by passage of wakes shed from rotating blades with a rotational velocity  $\omega r$ . Assume the wakes to be nonoverlapping so that a single wake (for simplicity taken as symmetric) relative to the blade is given as shown in Fig. 11. To determine the onset flow  $V$  and the angle of attack  $\alpha$  with respect of the stationary cylinder as a function of time, we observe that the onset flow velocity relative to the moving cylinder is  $V_R$  and that the cylinder sheds a wake whose velocity distribution parallel to the  $V_R$ -direction is given by

$$V_1 = V_R f\left(\frac{y}{\delta}\right)$$

Here  $y$  denotes the distance normal to  $V_R$  and  $\delta$  the wake half-width. The velocity in the wake with respect to the stationary cylinder,  $V$ , can then be obtained by subtracting the rotational speed  $\omega r$  from  $V_1$  as shown in Fig. A1. In terms of known quantities, it follows from Fig. A1 that

$$\frac{V}{V_\infty} = \left[ f^2 + \frac{\omega^2 r^2}{V_\infty^2} (1 - f)^2 \right]^{1/2} \quad (\text{A-1})$$

$$\tan \alpha = \frac{\omega r}{V_\infty} \left( \frac{1 - f}{f} \right) \quad (\text{A-2})$$

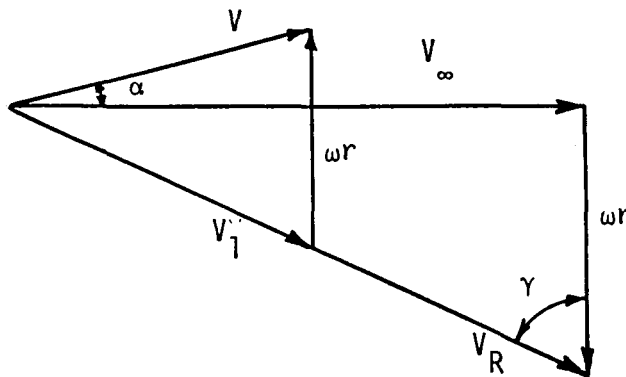


Figure A1. Sketch of velocity vectors behind a moving blade row.

To apply Eqs. (A-1) and (A-2) to the stagnation point solution on the circular cylinder, we make further simplifying assumptions as follows: although Eqs.

(A-1) and (A-2) represent a variable onset flow for the whole cylinder, we take the stagnation point location to be determined by the angle  $\alpha$ , or that  $\theta = \alpha$  on the cylinder periphery, and let the instantaneous onset flow be equal to  $V$ . This is clearly a quasi-steady approach which becomes more accurate as the ratio of the cylinder diameter with respect to the wake width decreases. By analogy to the steady-state flow around the stagnation point, we write for the velocity at each instant

$$u_e = \frac{4V}{D} (X - X_0) \quad (A-3)$$

where  $X_0$  is the stagnation point location with respect to  $\alpha = \theta = 0$ . Inserting Eqs. (A-1) and (A-2) into Eq. (A-3), we obtain:

$$\frac{u_e}{V_\infty} = 2 \left[ f^2 + \frac{\omega^2 r^2}{V_\infty^2} (1-f)^2 \right]^{1/2} \left\{ \frac{2X}{D} - \tan^{-1} \left[ \frac{\omega r}{V_\infty} \left( \frac{1-f}{f} \right) \right] \right\} \quad (A-4)$$

For a symmetrical wake, the nondimensional velocity distribution  $f$  may be represented by:

$$f\left(\frac{Y}{\delta}\right) = 1 - 0.976 \left(\frac{C_D^d}{S}\right)^{1/2} \left[ 1 - \left| \frac{Y}{\delta} \right|^{3/2} \right]^2 \quad (A-5)$$

Here  $C_D^d$  is the drag area of the blade and  $S$  is the distance from the blade to the cylinder. Equation (A-5) can also be approximated by

$$f\left(\frac{Y}{\delta}\right) = \frac{1 + V_m}{2} - \frac{1 - V_m}{2} \cos \pi \left(\frac{Y}{\delta}\right)$$

with  $V_m$  denoting the nondimensional centerline velocity given by

$$V_m = 1 - 0.976 \left(\frac{C_D^d}{S}\right)^{1/2}$$

To introduce time dependence, we observe that the wake width  $W$  in the plane of rotation of the cylinder is:

$$W = \frac{2\delta}{\sin \gamma} = \frac{2\delta V_R}{V_\infty} \quad (A-6)$$

Since one wake covers  $\delta V_R / \pi r V_\infty$  of the periphery, the period  $t_w$  for one wake to pass is:

$$t_w = \frac{2\delta V_R}{r \omega V_\infty} = \frac{2\delta}{V_\infty} \frac{[1 + (\omega r / V_\infty)^2]^{1/2}}{(\omega r / V_\infty)} \quad (A-7)$$

If there are  $n$  blades, the period  $t_g$  for one gap is

$$t_g = \frac{2\pi}{n\omega} - t_w \quad (\text{A-8a})$$

or in terms of the blade passing frequency  $F$

$$F = \frac{n\omega}{2\pi} \quad (\text{A-8b})$$

The full width of the wake,  $2\delta$ , is given by

$$2\delta = 1.132(C_D d S)^{1/2} \quad (\text{A-9})$$

It takes time  $t_w$  to travel across the wake of distance  $2\delta$ , so that in time  $t$ , the normal distance traveled is:

$$\bar{y} = \frac{2\delta t}{t_w} \quad (\text{A-10})$$

Here  $\bar{y}$  is measured from the edge of the wake

$$\bar{y} = \delta - y \quad (\text{A-11})$$

so that:

$$\frac{y}{\delta} = 1 - \frac{\bar{y}}{\delta} = 1 - \frac{2t}{t_w} \quad 0 \leq t \leq t_w \quad (\text{A-12})$$

In terms of the relations defined by Eqs. (A-7), (A-9), (A-10) and (A-11), and with the definition of Strouhal number  $St$ , Eq. (A-12) can also be written as

$$\frac{y}{\delta} = 1 - E_1 \frac{\tau St}{[1 + E_2^2 St^2]^{1/2}} \quad (\text{A-13})$$

where  $\tau$  is a dimensionless time

$$\tau = \frac{V_\infty t}{D} \quad (\text{A-14a})$$

and the parameters  $E_1$  and  $E_2$  are defined by

$$E_1 = \frac{2\pi}{1.132n(C_D d/D S/D)^{1/2}}, \quad E_2 = \frac{2\pi r}{nD} \quad (\text{A-14b})$$

Noting that  $f$  is a function of  $\tau$  and that Eq. (A-4) is of the form given by Eq. (1), we can represent the external velocity distribution near the stagnation region of the circular cylinder with  $u_\infty = 2V_\infty$ ,  $\xi = 2x/D = x/r$ ,  $St = (n/\pi)(\omega r/V_\infty)$  by defining A and B as

$$A(\xi, \tau) = [f^2 + E_2 (St)^2 (1 - f)^2]^{1/2} \quad (A-15)$$

$$B(\tau) = \tan^{-1} [E_2 St (\frac{1-f}{f})] \quad (A-16)$$

$$f(\tau) = \frac{1 + V_m}{2} + \frac{1 - V_m}{2} \cos [\pi (y/\delta)] \quad (A-17)$$

with  $y/\delta$  in Eq. (A-17) given by Eq. (A-13).

As we can see from Eqs. (A-15), (A-16) and (A-17), an expression of the form given by Eq. (1) can be obtained for the stagnation region of the cylinder as a function of  $St$  by assigning values to  $E_1$ ,  $E_2$  and  $V_m$ . This can be done for both laminar and turbulent flows as discussed in Section 4.3.



## Report Documentation Page

<b>1. Report No.</b> NASA CR-4206	<b>2. Government Accession No.</b> 	<b>3. Recipient's Catalog No.</b> 	
<b>4. Title and Subtitle</b> A General Method for Unsteady Heat Transfer on Turbine Blades		<b>5. Report Date</b> January 1989	
		<b>6. Performing Organization Code</b> 	
<b>7. Author(s)</b> Tuncer Cebeci and Max F. Platzer		<b>8. Performing Organization Report No.</b> None (E-4491)	
		<b>10. Work Unit No.</b> 582-01-11	
<b>9. Performing Organization Name and Address</b> Naval Postgraduate School Department of Aeronautics Monterey, California 93943		<b>11. Contract or Grant No.</b> C-80017-F	
		<b>13. Type of Report and Period Covered</b> Contractor Report Final	
<b>12. Sponsoring Agency Name and Address</b> National Aeronautics and Space Administration Lewis Research Center Cleveland, Ohio 44135-3191		<b>14. Sponsoring Agency Code</b> 	
		<b>15. Supplementary Notes</b> Project Manager, James E. O'Brien, Internal Fluid Mechanics Division, NASA Lewis Research Center. Tuncer Cebeci, Aerospace Engineering Department, California State University, Long Beach, California; Max F. Platzer, Department of Aeronautics, Naval Postgraduate School, Monterey, California.	
<b>16. Abstract</b> <p>This report is concerned with the development of a general method for calculating unsteady heat transfer on turbine blades. It is based on the numerical solution of the boundary-layer equations for laminar, transitional and turbulent flows. A novel procedure has been developed to account for the movement of the stagnation point caused by blade-passing wakes and has been applied to the stagnation region of three model flows with results which confirm its validity for laminar flows. It has also been applied to an experimental arrangement in which the average Nusselt number has been reported for turbulent flows and the results show considerable promise.</p>			
<b>17. Key Words (Suggested by Author(s))</b> Unsteady heat transfer Boundary layers Turbine		<b>18. Distribution Statement</b> Unclassified - Unlimited Subject Category 34	
<b>19. Security Classif. (of this report)</b> Unclassified	<b>20. Security Classif. (of this page)</b> Unclassified	<b>21. No of pages</b> 40	<b>22. Price*</b> A03